Mineralogical Magazine (2021), **85**, 379–386
doi:10.1180/mgm.2021.26

CAMBRIDGE
UNIVERSITY PRESS

Article

Thebaite-(NH_4), $(NH_4,K)_3Al(C_2O_4)(PO_3OH)_2(H_2O)$, a new phosphate–oxalate mineral from the Rowley mine, Arizona, USA

Anthony R. Kampf[1]*, Mark A. Cooper[2], Aaron J. Celestian[1], Barbara P. Nash[3] and Joe Marty[4]

[1]Mineral Sciences Department, Natural History Museum of Los Angeles County, 900 Exposition Boulevard, Los Angeles, California 90007, USA; [2]Department of Geological Sciences, University of Manitoba, Winnipeg, Manitoba, R3T 2N2, Canada; [3]Department of Geology and Geophysics, University of Utah, Salt Lake City, Utah 84112, USA; and [4]5199 East Silver Oak Road, Salt Lake City, Utah 84108, USA

Abstract

Thebaite-(NH_4), $(NH_4,K)_3Al(C_2O_4)(PO_3OH)_2(H_2O)$, is a new mineral species (IMA2020-072) from the Rowley mine, Maricopa County, Arizona, USA. It occurs in an unusual bat-guano-related, post-mining assemblage of phases that include a variety of vanadates, phosphates, oxalates and chlorides, some containing NH_4^+. Other secondary minerals found in association with thebaite-(NH_4) are antipinite, vanadinite and at least one other new mineral. Crystals of thebaite-(NH_4) are colourless blades up to ~0.1 mm in length. The streak is white, lustre is vitreous, Mohs hardness is 1½–2, tenacity is brittle and fracture is splintery. There are two good cleavages in the [010] zone, probably {100} and $\{10\bar{2}\}$. The calculated density is 2.093 $g \cdot cm^{-3}$. Thebaite-(NH_4) is optically biaxial (–) with $\alpha = 1.490(2)$, $\beta = 1.534(2)$, $\gamma = 1.570(2)$ (white light); $2V = 82.7(5)°$; slight $r > v$ dispersion; and orientation $X = \mathbf{b}$, $Y \wedge \mathbf{c} = 13°$ in obtuse β. Electron microprobe analysis gave the empirical formula $[(NH_4)_{2.12}K_{0.69}Na_{0.20}]_{\Sigma 3.01}(Al_{0.84}Fe^{3+}_{0.11}V^{3+}_{0.04})_{\Sigma 0.99}(C_2O_4)[(P_{0.98}Si_{0.02})O_3OH]_2(H_2O)$, with the C, N and H contents constrained by the crystal structure. Raman spectroscopy confirmed the presence of NH_4 and C_2O_4. Thebaite-(NH_4) is monoclinic, $P2_1/c$, with $a = 11.156(9)$, $b = 6.234(6)$, $c = 18.651(16)$ Å, $\beta = 102.928(15)°$, $V = 1264.2(19)$ Å^3 and $Z = 4$. The structural unit in the crystal structure of thebaite-(NH_4) ($R_1 = 0.0612$ for 863 $I_o > 2\sigma I$ reflections) is a double-strand chain of corner-sharing AlO_6 octahedra and PO_3OH tetrahedra decorated by additional PO_3OH tetrahedra and C_2O_4 groups. The decorated chains connect to one another through bonds to NH_4^+ and K^+ and through hydrogen bonds.

Keywords: thebaite-(NH_4), new mineral species, phosphate, oxalate, crystal structure, Rowley mine, Arizona

(Received 3 January 2021; accepted 10 March 2021; Accepted Manuscript published online: 16 March 2021; Associate Editor: Peter Leverett)

Introduction

The still actively forming bat guano assemblage at depth (125 feet) in the Rowley mine near Theba, Arizona has already proven to be a remarkable source of new minerals. Among these are the first minerals that contain both oxalate and phosphate groups: phoxite, $(NH_4)_2Mg_2(C_2O_4)(PO_3OH)_2(H_2O)_4$ (Kampf *et al.* 2019a) and davidbrownite-(NH_4), $(NH_4,K)_5(V^{4+}O)_2(C_2O_4)[PO_{2.75}(OH)_{1.25}]_4{\cdot}3H_2O$ (Kampf *et al.* 2019b). The new mineral described herein, thebaite-(NH_4), is the third known mineral containing both of these anionic groups, and several others are currently under study.

The mineral is named for Theba, Arizona, a small settlement and railroad depot ~20 km SE of the Rowley mine. At times in the past, the mine has been referred to as the Theba mine and, according to Wilson (2020), old labels on specimens from the mine often say "near Theba". For naming and species definition, the total occupancy of the three large cation sites in the structure is employed; thereby, the '-(NH_4)' suffix in the name reflects the fact that $NH_4^+ > K^+$. If an analogue with $K^+ > NH_4^+$ were found, it would be named thebaite-(K).

The new mineral and name were approved by the Commission on New Minerals, Nomenclature and Classification of the International Mineralogical Association (IMA2020-072, Kampf *et al.* 2021). The holotype specimen of thebaite-(NH_4) is deposited in the collections of the Natural History Museum of Los Angeles County, Los Angeles, California, USA, with catalogue number 75082.

Occurrence

Thebaite-(NH_4) was found on the 125-foot level of the Rowley mine (33°2′57″N, 113°1′49.59″W), ~20 km NW of Theba (small settlement and railroad depot), Maricopa County, Arizona, USA. The Rowley mine is on the western slope of the Painted Rock Mountains (in the Painted Rock mining district) and overlooks the Dendora Valley, immediately to the west. It is a former Cu–Pb–Au–Ag–Mo–V–baryte–fluorspar mine that exploited veins presumed to be related to the intrusion of an andesite porphyry dyke into Tertiary volcanic rocks. Although the mine has not been operated for ore since 1923, collectors took notice of the mine as a source of fine wulfenite crystals in ~1945. An up-to-date account of the history, geology and mineralogy of the mine was published recently by Wilson (2020).

The new mineral was found in a hot and humid area of the mine (see figure 26 in Wilson, 2020) in an unusual bat-guano-related, post-mining assemblage of phases that include

---

*Author for correspondence: Anthony R. Kampf, E-mail: akampf@nhm.org

Cite this article: Kampf A.R., Cooper M.A., Celestian A.J., Nash B.P. and Marty J. (2021) Thebaite-(NH_4), $(NH_4,K)_3Al(C_2O_4)(PO_3OH)_2(H_2O)$, a new phosphate–oxalate mineral from the Rowley mine, Arizona, USA. *Mineralogical Magazine* **85**, 379–386. https://doi.org/10.1180/mgm.2021.26

Fig. 1. Sprays of thebaite-(NH_4) blades; field of view 0.6 mm across. Holotype, catalogue number 75082.

a variety of vanadates, phosphates, oxalates and chlorides, some containing NH_4^+. This secondary mineral assemblage is found growing on baryte-quartz-rich matrix and, besides thebaite-(NH_4) includes allantoin (Kampf *et al.*, 2020), ammineite, antipinite, aphthitalite, bassanite, biphosphammite, cerussite, davidbrownite-(NH_4) (Kampf *et al.*, 2019a), fluorite, halite, hydroglauberite, mimetite, mottramite, natrosulfatourea (Kampf *et al.*, 2020), perite, phoxite (Kampf *et al.*, 2019b), quartz, rowleyite (Kampf *et al.*, 2017), salammoniac, struvite, thénardite, urea, vanadinite, weddellite, willemite, wulfenite and several other potentially new minerals. Thebaite-(NH_4) was found in intimate association with antipinite, vanadinite and at least one other new mineral.

Physical and optical properties

Crystals of thebaite-(NH_4) are colourless blades, up to ~0.1 mm in length, often growing in sprays (Fig. 1). The blades are elongate on [010], flattened on {001} and exhibit the crystal forms {100}, {001} and {320} (Fig. 2). Possible twinning on {100} was observed under crossed polars. The streak is white, the lustre is vitreous, the Mohs hardness is between 1½ and 2, the tenacity is brittle and the fracture is splintery. There are two good cleavages in the [010] zone, probably {100} and {10$\bar{2}$}. The tiny crystals are virtually invisible in density liquids making the measurement of their density impossible. The calculated density is 2.093 g·cm^{-3} using the empirical formula and 1.991 g·cm^{-3} using the ideal (NH_4 end-member) formula. Thebaite-(NH_4) is non-fluorescent in long- and short-wave ultraviolet light. The mineral is insoluble at room temperature in H_2O, but easily soluble in dilute HCl.

Thebaite-(NH_4) is optically biaxial (–) with $\alpha = 1.490(2)$, $\beta = 1.534(2)$ and $\gamma = 1.570(2)$ determined in white light. The 2V measured using extinction data with *EXCALIBR* (Gunter *et al.*, 2004) is 82.7(5)° and the calculated 2V is 82.0°. Slight $r > v$ dispersion was observed. The optical orientation is $X = \mathbf{b}$, $Y \wedge \mathbf{c} = 13°$ in the obtuse angle β. The mineral is non-pleochroic.

Raman spectroscopy

Raman spectroscopy was conducted on a Horiba XploRA PLUS using a 532 nm diode laser, 100 μm slit and 2400 gr/mm diffraction grating and a 100× (0.9 NA) objective. The spectrum from 4000 to 60 cm^{-1} is shown in Fig. 3. Full pattern peak fitting was performed using a least-squares approach using Gaussian peak shapes to minimise the difference between measured and calculated profiles, and cubic-spline was used for base-line modelling.

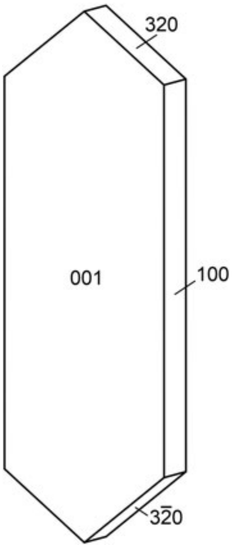

Fig. 2. Crystal drawing of thebaite-(NH_4); clinographic projection in non-standard orientation, **b** vertical.

Both O–H and N–H stretching are manifest as bands in the 3600–2800 cm^{-1} range (Colmenero, 2019) and definitive distinction between them in this and other regions is not possible. The assignment of most of the other bands can be made by reference to the spectrum of phoxite, $(NH_4)_2Mg_2(C_2O_4)(PO_3OH)_2(H_2O)_4$ (Kampf *et al.*, 2019) and other oxalate minerals (e.g. weddellite, wheatleyite, moolooite, natroxalate, oxammite and glushinskite) (Frost, 2004, 2008) (Peterson and Pullman, 2016) as described below.

The Raman bands at 1722 cm^{-1} and 1679 cm^{-1} are related to H–N–H bending, while the lower wavenumber shoulder at 1631 cm^{-1} is related to the asymmetric stretching of C=O. The moderately strong Raman band at 1464 cm^{-1} is related to a combination of C–O symmetric stretch, and very weak bands at 1418 cm^{-1} and 1311 cm^{-1} may be related to O–C–O wagging in the oxalate group, although it also occurs in a region in which O–H and H–N–H bending is manifest. The bands at 1157 cm^{-1} and 1102 cm^{-1} are C–O stretching plus out-of-plane deformation bending of O–C=O. The PO_3OH asymmetric stretch and the PO_3OH symmetric stretch were observed at 1053 cm^{-1} and 998 cm^{-1}, respectively; the 912 cm^{-1} band is probably also related to PO_3OH stretching. The origin of the broad band between 636 cm^{-1} and 551 cm^{-1} is uncertain, but it could be related to O–P–O bending combined with C–C bending. Bands between 405 cm^{-1} and 60 cm^{-1} are assigned as lattice modes.

Chemical analysis

Analyses of thebaite-(NH_4) (3 points) were done at the University of Utah on a Cameca SX-50 electron microprobe with four wavelength dispersive spectrometers using Probe for EPMA software. Analytical conditions were 15 kV accelerating voltage, 10 nA beam current and a beam diameter of 5 μm. Raw X-ray intensities

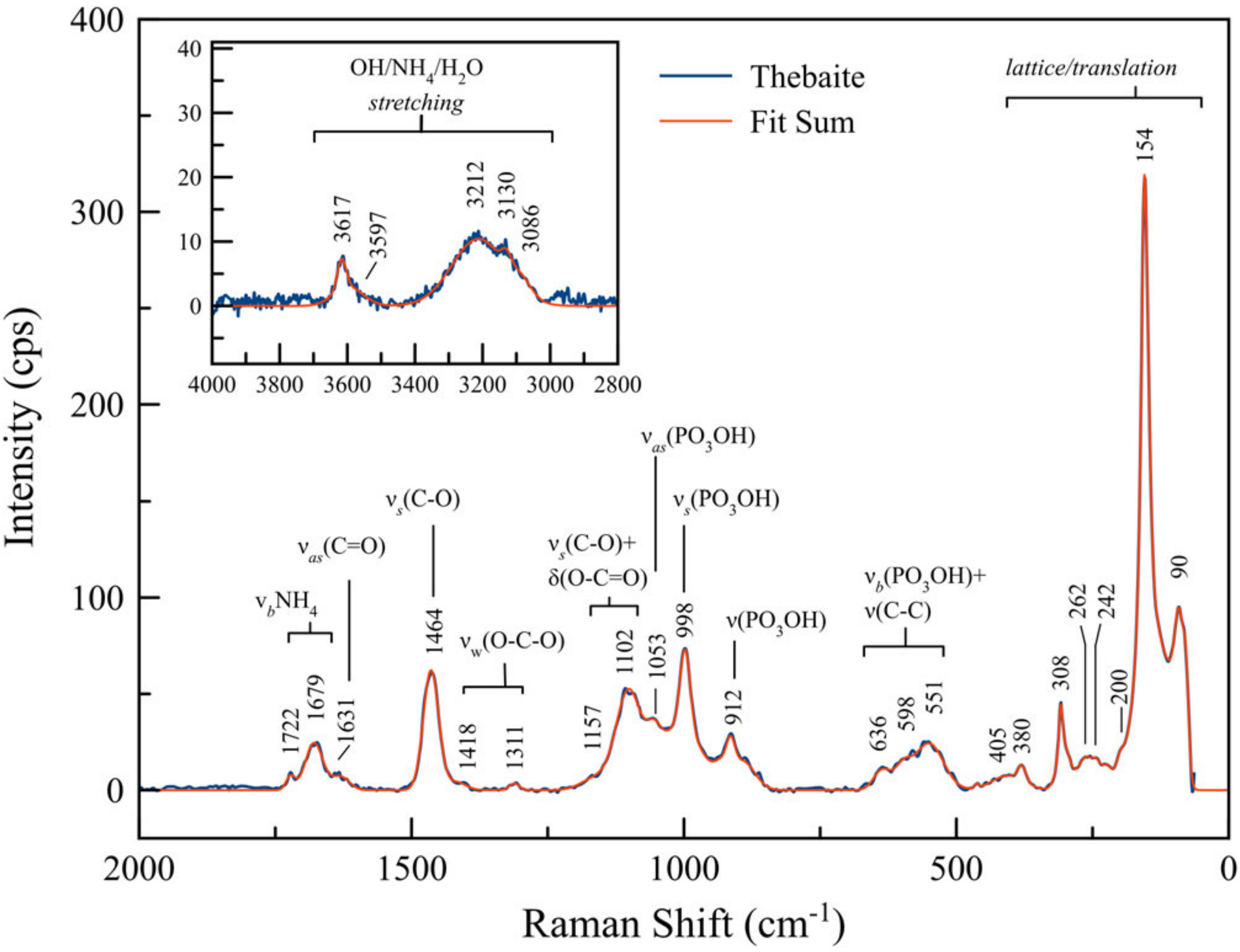

Fig. 3. Raman spectrum of thebaite-(NH_4).

were corrected for matrix effects with a ϕρ(z) algorithm (Pouchou and Pichoir, 1991). Na and K intensities were corrected for time-dependent decreases in intensity during analyses. Severe damage from the electron beam was observed. Attempts to analyse N (syn. Cr_2N standard) provided values much lower than those predicted by the structure refinement. The low values for N [$(NH_4)_2O$] by EPMA are probably due to loss of most of the NH_4 under vacuum and especially resulting from beam damage. Because insufficient material is available for CHN analyses, C_2O_3, H_2O and $(NH_4)_2O$ were calculated based upon the structure determination. Note that the structure indicates $NH_4 + K + Na = 3$ atoms per formula unit (apfu), and this is the basis for the calculated $(NH_4)_2O$ value. The high analytical total is probably due to the partial loss of NH_4 and H_2O under vacuum and due to beam damage, which results in higher concentrations for the remaining constituents. Analytical data are given in Table 1.

The empirical formula (based on P + Si = 2 and O = 13 apfu) is $[(NH_4)_{2.12}K_{0.69}Na_{0.20}]_{\Sigma 3.01}(Al_{0.84}Fe^{3+}_{0.11}V^{3+}_{0.04})_{\Sigma 0.99}(C_2O_4)[(P_{0.98}Si_{0.02})O_3OH]_2(H_2O)$ (+0.05 H for charge balance. The simplified formula is $(NH_4,K,Na)_3(Al,Fe^{3+},V^{3+})(C_2O_4)(PO_3OH)_2(H_2O)$ and the ideal (NH_4 end-member) formula is $(NH_4)_3Al(C_2O_4)(PO_3OH)_2(H_2O)$, which requires $(NH_4)_2O$ 20.61, Al_2O_3 13.45, P_2O_5 37.44, C_2O_3 19.00, H_2O 9.50, total 100 wt.%. The Gladstone–Dale compatibility (Mandarino, 2007) 1 – (K_p/K_c) is 0.029 in the range of excellent compatibility for the empirical formula.

Table 1. Analytical data (wt.%) for thebaite-(NH_4).

Constituent	Mean	Min.	Max.	S.D.	Probe standard	Normalised
$(NH_4)_2O$*	7.03	6.14	7.91	0.89	Cr_2N	13.84
K_2O	12.06	11.29	13.30	1.08	sanidine	8.10
Na_2O	2.27	1.71	2.91	0.60	albite	1.52
Al_2O_3	16.09	15.00	17.01	1.02	sanidine	10.81
Fe_2O_3	3.19	2.54	3.62	0.57	hematite	2.14
V_2O_3	1.10	0.97	1.19	0.12	V metal	0.81
SiO_2	0.48	0.35	0.56	0.11	albite	0.32
P_2O_5	52.47	49.27	56.84	3.92	apatite	35.24
C_2O_3*						18.07
H_2O*						9.15
Total						100.00

*$(NH_4)_2O$, C_2O_3 and H_2O values in the Normalised column are based on the structure.
S.D. – standard deviation

X-ray crystallography and structure determination

Powder X-ray studies were done using a Rigaku R-Axis Rapid II curved imaging plate microdiffractometer with monochromatised MoKα radiation. A Gandolfi-like motion on the φ and ω axes was

Table 2. Data collection and structure refinement details for thebaite-(NH_4).

Crystal data	
Refined formula	$(NH_4)_{1.62}K_{1.04}Na_{0.33}Al_{0.90}Fe^{3+}_{0.10}C_2P_{1.88}O_{12.76}$
Space group	$P2_1/c$
Unit cell dimensions	$a = 11.156(9)$ Å
	$b = 6.234(6)$ Å
	$c = 18.651(16)$ Å
	$\beta = 102.927(15)°$
V	1264.2(19) $Å^3$
Z	4
Density (calculated)	2.036 $g \cdot cm^{-3}$
Absorption coefficient	0.930 mm^{-1}
F(000)	765.9
Data collection	
Diffractometer	Bruker D8 three-circle; multilayer optics; APEX-II CCD
Temperature	293(2) K
X-ray radiation / source	Mo$K\alpha$ ($\lambda = 0.71073$ Å) / rotating anode
Crystal size	70 × 13 × 4 μm
θ range for data collection	3.23 to 22.71°
Reflections collected	6266
Independent reflections	1679 [$R_{int} = 0.17$]
Reflections with $I_o > 2\sigma I$	863
Completeness to θ = 22.71°	99.1%
Index ranges	$-12 \le h \le 12$, $-6 \le k \le 6$, $-20 \le l \le 20$
Refinement	
Refinement method	Full-matrix least-squares on F^2
Parameters / restraints	195 / 0
Goodness-of-fit on F^2	1.017
Final R indices [$I > 2\sigma(I)$]	$R_1 = 0.0612$, $wR_2 = 0.1363$
R indices (all data)	$R_1 = 0.1461$, $wR_2 = 0.1720$
Largest diff. peak and hole	0.80 and –0.42 e^-/A^3

*$R_{int} = \Sigma|F_o^2 - F_o^2(\text{mean})|/\Sigma[F_o^2]$. GoF = $S = \{\Sigma[w(F_o^2 - F_c^2)^2]/(n-p)\}^{½}$. $R_1 = \Sigma||F_o| - |F_c||/\Sigma|F_o|$. $wR_2 = \{\Sigma[w(F_o^2 - F_c^2)^2]/\Sigma[w(F_o^2)^2]\}^{½}$; $w = 1/[\sigma^2(F_o^2) + (aP)^2 + bP]$ where a is 0.081, b is 0 and P is $[2F_c^2 + \text{Max}(F_o^2, 0)]/3$.

used to randomise the sample. Observed *d* values and intensities were derived by profile fitting using *JADE Pro* software (Materials Data, Inc.). The powder data are presented in Supplementary Table S1. Unit-cell parameters refined from the powder data using *JADE Pro* with whole pattern fitting are $a = 11.12(3)$, $b = 6.27(3)$, $c = 18.74(2)$ Å, $\beta = 103.54(9)°$ and $V = 1270(7)$ $Å^3$.

Single-crystal X-ray studies were done using a Bruker D8 three-circle diffractometer equipped with a rotating anode generator (Mo$K\alpha$ X-radiation), multilayer optics and an APEX-II CCD area detector. A total of 23,373 reflections (6268 in the Ewald sphere) were integrated using 64s frames with a 0.3° frame width. The unit-cell dimensions were obtained by least-squares refinement of 1521 reflections with $I_o > 7\sigma I$. Systematically absent reflections are consistent with the space group $P2_1/c$. Careful visual inspection of frames confirmed that all reflections were consistent with this cell and space group. Empirical absorption corrections (*SADABS*, Bruker AXS) were applied and equivalent reflections were merged. The structure was solved by direct methods using *SHELXS-2013* and the structure was refined using *SHELXL-2016* (Sheldrick, 2015). All atoms were refined with anisotropic displacement parameters. H atom sites could not be reliably extracted from the difference-Fourier map.

Of the three large cation sites, K has the smallest average bond length along with three distinctively shorter (~2.68 Å) individual bonds, and Na is presumed to order at this site; hence, the refined scattering was modelled with coupled K and Na scattering factors (site K is K dominant, in agreement with the chemical analysis, Tables 1, 4). The other two large cation sites (N1 and N2) have significantly less relative scattering and were modelled with coupled K and N scattering factors (both are NH_4 dominant, Table 4). The Al site exhibited greater scattering than expected for Al alone, so it was modelled with coupled Al and Fe; refined site-scattering in close agreement with minor Fe and V measured chemically. There are two P sites; The P1 site and its coordinated O sites are fully occupied; however, the P2 site-scattering reveals a significant deficiency from full occupation by P. Of the four O sites coordinated to P2 (OH5, O6, O7 and O8), O6 and O8 also exhibit scattering deficiency, while OH5 and O7 appear to be fully occupied; in the final refinement cycles, the occupancies of the P2, O6 and O8 sites were jointly refined to 0.879(9) occupancy. An H_2O site was located, but because of the highly prolate shape of its ellipsoid when refined anisotropically, it was refined as a split site (OWA and OWB separated by 0.66(4) Å and refined isotropically) with a total occupancy of 1.0. The occupancy

Table 3. Atom positions, occupancy and displacement parameters ($Å^2$) for thebaite-(NH_4).

	Occupancy	x/a	y/b	z/c	U_{eq}	U^{11}	U^{22}	U^{33}	U^{23}	U^{13}	U^{12}
K	$K_{0.67}Na_{0.33(2)}$	0.8845(2)	0.2489(6)	0.61514(14)	0.0521(13)	0.0237(15)	0.081(3)	0.0488(19)	0.0095(17)	0.0022(11)	−0.0072(17)
N1	$(NH_4)_{0.784}K_{0.216(14)}$	0.5148(5)	0.3750(11)	0.6664(3)	0.052(3)	0.050(4)	0.052(5)	0.053(4)	0.000(3)	0.011(3)	0.001(3)
N2	$(NH_4)_{0.837}K_{0.163(17)}$	0.8162(7)	0.2278(13)	0.3420(4)	0.075(4)	0.082(6)	0.071(7)	0.073(6)	0.013(4)	0.019(4)	0.009(5)
P1	P	0.61541(18)	0.2443(5)	0.49820(12)	0.0234(7)	0.0206(12)	0.0195(13)	0.0305(13)	−0.0015(15)	0.0067(9)	−0.0021(16)
P2	$P_{0.879(9)}$	0.3213(3)	0.1426(5)	0.30268(16)	0.0322(11)	0.042(2)	0.031(2)	0.0221(18)	−0.0011(15)	0.0046(13)	−0.0056(16)
Al	$Al_{0.898}Fe_{0.102(10)}$	0.31772(18)	0.2552(5)	0.46769(12)	0.0211(9)	0.0187(13)	0.0151(15)	0.0287(14)	−0.0025(13)	0.0040(9)	−0.0009(14)
C1	C	0.1697(9)	0.2593(17)	0.5650(5)	0.031(2)	0.050(7)	0.026(6)	0.019(5)	−0.002(5)	0.009(4)	−0.004(7)
C2	C	0.0802(9)	0.2561(18)	0.4897(5)	0.031(2)	0.042(6)	0.026(6)	0.028(5)	−0.003(6)	0.014(5)	0.005(6)
OH1	OH	0.6093(5)	0.2382(11)	0.4128(3)	0.0339(16)	0.033(3)	0.039(4)	0.030(3)	0.006(4)	0.008(3)	0.001(4)
O2	O	0.6888(6)	0.4409(10)	0.5287(3)	0.0307(18)	0.026(4)	0.022(4)	0.042(4)	−0.001(3)	0.004(3)	0.001(3)
O3	O	0.4852(4)	0.2516(11)	0.5100(3)	0.0257(14)	0.016(3)	0.024(3)	0.040(3)	−0.006(3)	0.011(2)	0.002(3)
O4	O	0.6862(6)	0.0500(10)	0.5341(3)	0.0278(17)	0.019(4)	0.018(4)	0.045(4)	0.000(3)	0.004(3)	0.006(3)
OH5	OH	0.3030(7)	0.3015(13)	0.2364(4)	0.065(3)	0.069(5)	0.071(8)	0.048(5)	0.017(4)	0.000(4)	−0.014(5)
O6	$O_{0.879(9)}$	0.4501(7)	0.0477(14)	0.3104(4)	0.045(2)	0.043(5)	0.049(6)	0.046(5)	−0.009(4)	0.018(4)	0.006(4)
O7	O	0.3208(5)	0.2761(11)	0.3688(3)	0.0351(18)	0.041(4)	0.040(5)	0.025(4)	0.003(3)	0.008(3)	−0.009(4)
O8	$O_{0.879(9)}$	0.2227(8)	0.9744(14)	0.2852(4)	0.049(3)	0.061(6)	0.046(6)	0.038(5)	−0.006(4)	0.004(4)	−0.029(5)
O9	O	0.2813(5)	0.2537(11)	0.5648(3)	0.0309(15)	0.021(3)	0.040(4)	0.032(4)	0.001(3)	0.005(3)	0.001(4)
O10	O	0.1269(6)	0.2656(13)	0.6210(4)	0.050(2)	0.035(4)	0.078(6)	0.038(4)	−0.002(4)	0.010(3)	0.004(5)
O11	O	0.1352(5)	0.2536(11)	0.4371(3)	0.0332(16)	0.030(3)	0.029(4)	0.039(4)	0.001(4)	0.005(3)	0.002(4)
O12	O	0.9678(5)	0.2520(13)	0.4832(3)	0.0433(18)	0.021(4)	0.061(5)	0.048(4)	0.002(4)	0.009(3)	−0.001(5)
OWA	$(H_2O)_{0.61(10)}$	0.986(3)	0.472(4)	0.756(2)	0.098(11)						
OWB	$(H_2O)_{0.39(10)}$	0.946(5)	0.507(6)	0.726(4)	0.089(17)						

Table 4. Selected bond lengths (Å) for thebaite-(NH_4).

K–OWB$_{(0.39)}$	2.59(5)	N1–O6	2.685(11)	N2–O8$_{(0.88)}$	2.779(11)
K–O10	2.684(7)	N1–O9	2.957(8)	N2–O12	2.797(10)
K–O4	2.687(7)	N1–O3	2.962(8)	N2–OH1	2.905(9)
K–O2	2.687(7)	N1–O6$_{(0.88)}$	2.971(9)	N2–OWA$_{(0.61)}$	3.01(2)
K–O8$_{(0.88)}$	2.796(8)	N1–OH1	3.000(9)	N2–OH5	3.179(11)
K–O12	2.819(7)	N1–O7	3.011(9)	N2–O10	3.185(12)
K–OWA$_{(0.61)}$	2.96(4)	N1–OH5	3.136(10)	N2–OWB$_{(0.39)}$	3.20(4)
K–OWA$_{(0.61)}$	3.05(3)	N1–OH5	3.143(10)	N2–O10	3.265(12)
K–O11	3.243(8)	<N1–O>	2.983	<N2–O>	3.040
K–O11	3.274(8)				
<K–O>	2.879	P1–O2	1.513(7)	C1–C2	1.530(13)
		P1–O4	1.517(7)	C1–O10	1.242(10)
Al–O7	1.857(6)	P1–O3	1.518(5)	C1–O9	1.247(10)
Al–O3	1.859(5)	P1–OH1	1.579(6)	C2–O12	1.233(10)
Al–O2	1.898(7)	<P1–O>	1.532	C2–O11	1.268(10)
Al–O4	1.903(7)				
Al–O9	1.942(6)	P2–O7	1.488(7)	Hydrogen bonds	
Al–O11	1.988(6)	P2–O8	1.502(8)	OH1···O6	2.588(10)
<Al–O>	1.918	P2–O6	1.531(8)	OH5···O10	2.604(10)
		P2–OH5	1.561(8)	OWA···O8	2.60(4)
		<P2–O>	1.521	OWA···OWB	3.00(5)

Subscripts in brackets are site occupancies.

deficient P2, O6 and O8 sites and the split H_2O site are discussed below. Data collection and refinement details are given in Table 3, atom coordinates and displacement parameters in Table 4, selected bond distances in Table 5 and a bond-valence analysis in Table 6. The crystallographic information file has been deposited with the Principal Editor of *Mineralogical Magazine* and is available as Supplementary material (see below).

The refinement clearly establishes the structure type, but suffers to some degree in precision due to poorer general data observation; mean I/σ for reflections ranges from ~18 (low 2θ) to ~1.5 (at resolution cut-off of 45°2θ). This poorer data observation is due to a combination of very low scattering (light element structure) and very small single-crystal volume. The very bright rotating anode X-ray source, combined with the long frame exposure, allowed for modest data observation out to an imposed resolution cut-off of 45°2θ. We note that about half of the unique data collected is observed ($I_o > 2\sigma I$) and that statistical measures (R values, merging of reflections) are somewhat elevated as a result.

Discussion of the structure

The structure of thebaite-(NH_4) includes three large cation sites coordinated by O (O, OH and/or H_2O) sites: K (nine-fold coordinated), N1 (eight-fold coordinated) and N2 (seven-fold coordinated). There is one Al site (octahedrally coordinated by O) and two P sites, P1 and P2, both tetrahedrally coordinated by three O and one OH. One oxalate (C_2O_4) group includes two independent C sites, C1 and C2 and four independent O sites.

The structural unit is a double-strand chain of corner-sharing AlO_6 octahedra and $P1O_3OH$ tetrahedra decorated by $P2O_3OH$ tetrahedra and C_2O_4 groups (Fig. 4). As noted above, the tetrahedral coordination surrounding the P2 site is formed by the OH5, O6, O7 and O8 sites; the occupancies of the P2, O6 and O8 sites refined jointly to an occupancy of 0.879. This appears to indicate a real deficiency in the $P2O_3(OH)$ tetrahedron. When this group is missing (12% of the time), the OH5 site would be an H_2O group and the O7 site would be an OH site. Furthermore, the aforementioned splitting of the H_2O site into OWA and OWB is probably related to the deficiency in the $P2O_3(OH)$ tetrahedron. It should be noted that the normalised EPMA data are consistent with full occupancy of the P sites; however, we do not regard the EPMA data to be of sufficient quality to draw definitive inferences regarding occupancies.

Without the decorating $P2O_3OH$ tetrahedra and C_2O_4 groups, the octahedral–tetrahedral double-strand chain in the structure of thebaite-NH_4 is topologically similar to chain components in several structures (Fig. 5). It is topologically identical to the chain in

Table 5. Bond-valences analysis for thebaite-(NH_4). Values are in valence units (vu).

	K	N1	N2	Al	P1	P2	C1	C2	H	Σ
OH1		0.12	0.15		1.12				0.70	2.09
O2	0.17			0.51	1.32					2.00
O3		0.13		0.56	1.30					1.99
O4	0.17			0.50	1.31					1.98
OH5		0.08 0.08	0.07			1.17$_{(\times 0.88\rightarrow)}$			0.72	1.98
O6		0.24$_{(\times 0.88\downarrow)}$ 0.11$_{(\times 0.88\downarrow)}$				1.26			0.30	1.91
O7		0.11		0.56		1.40$_{(\times 0.88\rightarrow)}$				1.90
O8	0.11$_{(\times 0.88\downarrow)}$		0.19$_{(\times 0.88\downarrow)}$			1.36			0.29	1.95
O9		0.13		0.45			1.46			2.04
O10	0.17		0.07 0.06				1.48		0.28	2.06
O11	0.04 0.04			0.40				1.39		1.87
O12	0.12		0.20					1.51		1.83
OWA	0.05$_{(\times 0.61\downarrow)}$ 0.04$_{(\times 0.61\downarrow)}$		0.07$_{(\times 0.61\downarrow)}$							
OWB	0.08$_{(\times 0.29\downarrow)}$		0.02$_{(\times 0.29\downarrow)}$							
C1								1.03		
C2							1.03			
Σ	0.98	1.00	0.84	3.10	5.05	5.19	3.97	3.93		

Bond-valence parameters for NH_4^+–O are from Garcia-Rodriguez *et al.* (2000); all others are from Gagné and Hawthorne (2015). Hydrogen bond valences based on $O_D\cdots O_A$ distances using the relation of Ferraris and Ivaldi (1988). The refined occupancies of all sites have been considered.

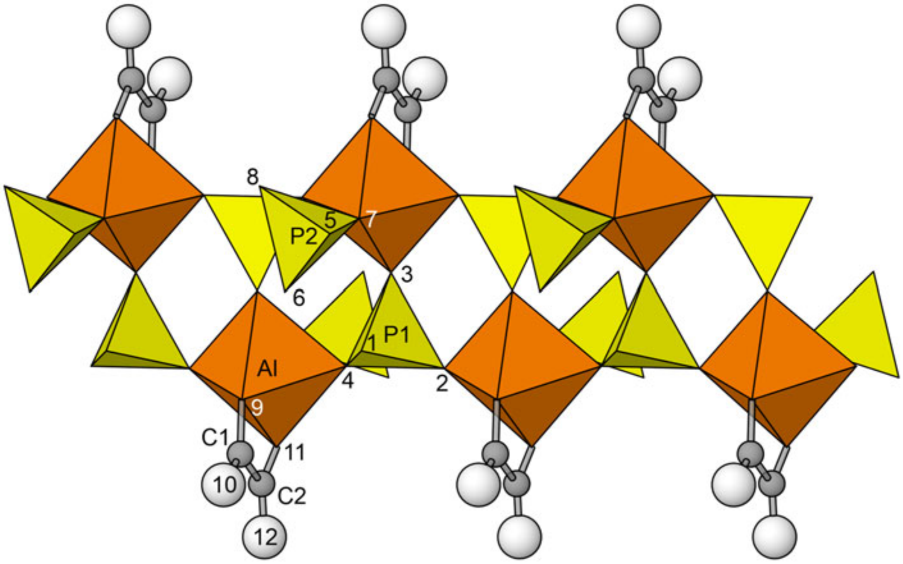

Fig. 4. The chain in the thebaite-(NH_4) structure along [010]. The O sites are numbered. [100] is vertical; [010] is canted down 20° from right to left.

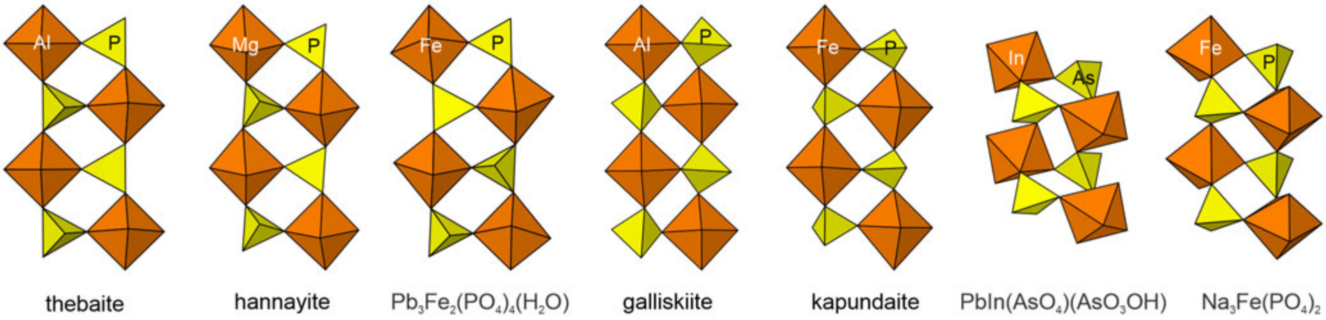

Fig. 5. Octahedral–tetrahedral double-strand chains in the structures of thebaite-(NH_4), hannayite, $Pb_3Fe_2(PO_4)_4(H_2O)$, galliskiite, kapundaite, $PbIn(AsO_4)(AsO_3OH)$ and $Na_3Fe(PO_4)_2$.

hannayite, $Mg_3(NH_4)_2(PO_3OH)_4·8H_2O$ (Catti and Franchini-Angela, 1976), while the chains in galliskiite, $Ca_4Al_2(PO_4)_2F_8·5H_2O$ (Kampf *et al.*, 2010), kapundaite, $(Na,Ca)_2Fe^{3+}_4(PO_4)_4(OH)_3·5H_2O$ (Mills *et al.*, 2010a) and synthetic $Pb_3Fe_2(PO_4)_4(H_2O)$ (Mills *et al.*, 2010b) are geometrical isomers. The octahedral–tetrahedral double-strand chains in synthetic $PbIn(AsO_4)(AsO_3OH)$ (Kolitsch and Schwendtner, 2005) and synthetic $Na_3Fe(PO_4)_2$ (Hatert, 2007) differ topologically from those in the aforementioned structures in that their octahedra share three corners of the same octahedral face with tetrahedra, while in all of the other chains, the octahedra share three equatorial corners with tetrahedra.

In thebaite-(NH_4), the chains, including the decorating components, connect to one another through bonds to the K site and the two NH_4 sites (N1 and N2) and through hydrogen bonds (Fig. 6). In contrast, the chains in hannayite connect to one another through decorating PO_4 tetrahedra corner-linked to intermediary FeO_6 octahedra to form sheets. The chains in kapundaite link directly to edge-sharing chains of FeO_6 octahedra, as well as to additional PO_4 tetrahedra to form a framework. In $Pb_3Fe_2(PO_4)_4(H_2O)$, two sets of interpenetrating chains are corner-linked into a framework. Other than thebaite-(NH_4), the only one of these structures with double-strand chain structural units is that of galliskiite in which the chains are undecorated and connect to one another *via* bonds to Ca cations.

Synthetic phases containing both phosphate and oxalate groups are often referred to as oxalatophosphates. In many of these phases, the phosphate and oxalate groups link with octahedrally coordinated cations to form porous frameworks with potential technological applications: catalysis, adsorption, ion exchange, gas storage, separation and sensing (Luan *et al.*, 2015). These structures take advantage of the oxalate group's ability to form strong bidentate linkages between octahedra. Such strong bidentate linkages between octahedra also occur in the structures of the other two oxalatophosphate minerals, phoxite, $(NH_4)_2Mg_2(C_2O_4)(PO_3OH)_2(H_2O)_4$ (Kampf *et al.*, 2019a) and davidbrownite-(NH_4), $(NH_4,K)_5(V^{4+}O)_2(C_2O_4)[PO_{2.75}(OH)_{1.25}]_4·3H_2O$ (Kampf *et al.*, 2019b), which both are found in the Rowley-mine guano mineral assemblage. The oxalate group in the thebaite-(NH_4) structure forms a bidentate linkage to a single AlO_6 octahedron, thereby decorating the double-strand chain rather than strongly linking it to other structural components. We are not aware of any synthetic phases with similarly decorated double-strand chains; however, another potentially new mineral in the Rowley-mine guano has a structural unit with an identical topology.

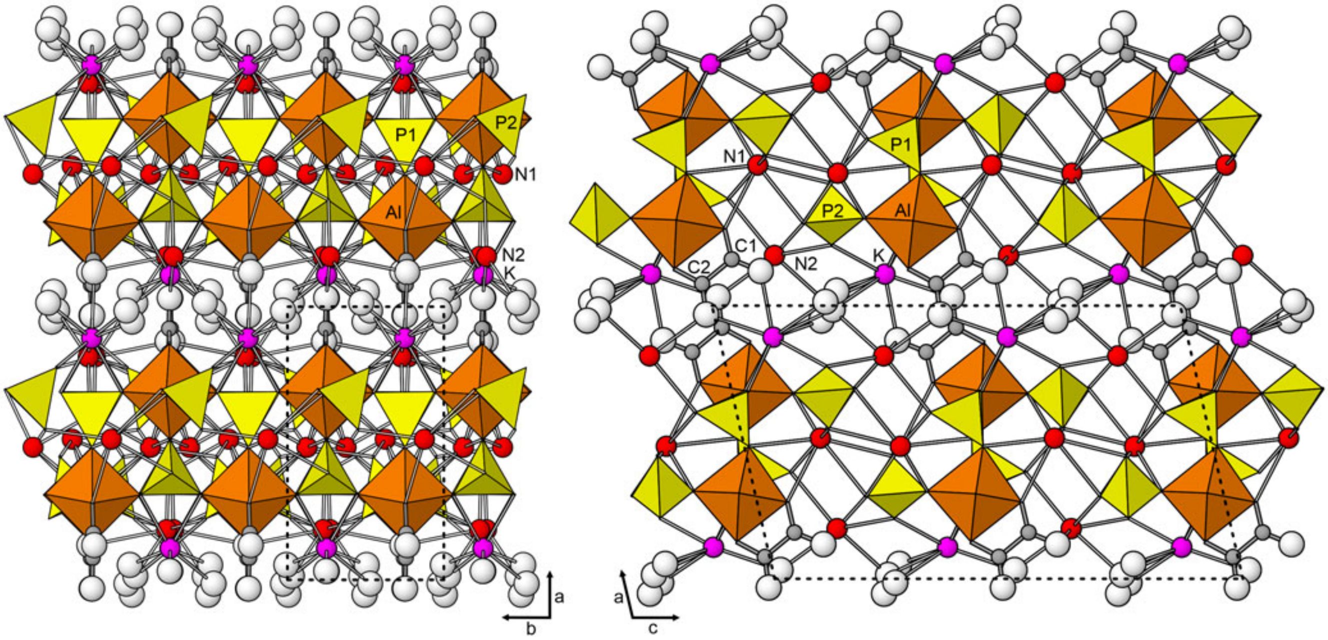

Fig. 6. The thebaite-(NH_4) structure viewed down [001] (left) and [010] (right). The unit-cell outline is shown with dashed lines.

Acknowledgements. Structural Editor Pete Leverett and two anonymous reviewers are thanked for constructive comments, which improved the manuscript. Keith Wentz, claim holder of the Rowley mine, is thanked for allowing underground access for the study of the occurrence and the collecting of specimens, along with Frank Hawthorne for providing access to the single-crystal instrument at the University of Manitoba. This study was funded, in part, by the John Jago Trelawney Endowment to the Mineral Sciences Department of the Natural History Museum of Los Angeles County.

Supplementary material. To view supplementary material for this article, please visit https://doi.org/10.1180/mgm.2021.26

References

Catti M. and Franchini-Angela M. (1976) Hydrogen bonding in the crystalline state. Structure of $Mg_3(NH_4)_2(HPO_4)_4(H_2O)_8$ (hannayite), and crystal chemical relationships with schertelite and struvite. *Acta Crystallographica*, **B32**, 2842–2848.

Colmenero F. (2019) Structural, spectroscopic, and thermodynamic characterization of ammonium oxalate monohydrate mineral using theoretical solid-state methods. *Journal of Physics and Chemistry of Solids*, **125**, 31–42.

Ferraris G. and Ivaldi G. (1988) Bond valence vs. bond length in O···O hydrogen bonds. *Acta Crystallographica*, **B44**, 341–344.

Frost R.L. (2004) Raman spectroscopy of natural oxalates. *Analytica Chimica Acta*, **517**, 207–214.

Frost R.L., Locke A. and Martens W.N. (2008) Synthesis and Raman spectroscopic characterisation of the oxalate mineral wheatleyite $Na_2Cu^{2+}(C_2O_4)_2\cdot 2H_2O$. *Journal of Raman Spectroscopy*, **39**, 901–908.

Gagné O.C. and Hawthorne F.C (2015) Comprehensive derivation of bond-valence parameters for ion pairs involving oxygen. *Acta Crystallographica*, **B71**, 562–578.

García-Rodríguez, L., Rute-Pérez, Á., Piñero, J.R. and González-Silgo, C. (2000) Bond-valence parameters for ammonium-anion interactions. *Acta Crystallographica*, **B56**, 565–569.

Gunter M.E., Bandli B.R., Bloss F.D., Evans S.H., Su S.C. and Weaver R. (2004) Results from a McCrone spindle stage short course, a new version of EXCALIBR, and how to build a spindle stage. *The Microscope*, **52**, 23–39.

Hatert F. (2007) Crystal structure of trisodium iron diphosphate, $Na_{2.88}Fe(PO_4)_2$, a synthetic phosphate with hannayite-type heteropolyhedral chains. *Zeitschrift für Kristallographie*, **222**, 6–8.

Kampf A.R., Colombo F., Simmons W.B., Falster A.U. and Nizamoff J.W. (2010) Galliskiite, $Ca_4Al_2(PO_4)_2F_8\cdot 5H_2O$, a new mineral from the Gigante granitic pegmatite, Córdoba province, Argentina. *American Mineralogist*, **95**, 392–396.

Kampf A.R., Cooper M.A., Nash B.P., Cerling T., Marty J., Hummer D.R., Celestian A.J., Rose T.P. and Trebisky T.J. (2017) Rowleyite, $[Na(NH_4,K)_9Cl_4][V_2^{5+,4+}(P,As)O_8]_6\cdot n[H_2O,Na,NH_4,K,Cl]$, a new mineral with a mesoporous framework structure. *American Mineralogist*, **102**, 1037–1044.

Kampf A.R., Celestian A.J., Nash B.P. and Marty J. (2019a) Phoxite, $(NH_4)_2Mg_2(C_2O_4)(PO_3OH)_2(H_2O)_4$, the first phosphate-oxalate mineral. *American Mineralogist*, **104**, 973–979.

Kampf A.R., Cooper M.A., Rossman R.R., Nash B.P., Hawthorne F.C. and Marty J. (2019b) Davidbrownite-(NH_4), $(NH_4,K)_5(V^{4+}O)_2(C_2O_4)[PO_{2.75}(OH)_{1.25}]_4\cdot 3H_2O$, a new phosphate-oxalate mineral from the Rowley mine, Arizona, USA. *Mineralogical Magazine*, **83**, 869–877.

Kampf A.R., Cooper M.A., Celestian A.J., Nash B.P. and Marty J. (2021) Thebaite-(NH_4), IMA 2020-072. CNMNC Newsletter 59; *Mineralogical Magazine*, **85**, 278–281.

Kolitsch U. and Schwendtner K. (2005) Octahedral–tetrahedral framework structures of $InAsO_4\cdot H_2O$ and $PbIn(AsO_4)(AsO_3OH)$. *Acta Crystallographica*, **C61**, i86–i89.

Luan L., Li J., Chen C., Lin Z. and Huang H. (2015) Solvent-free synthesis of crystalline metal phosphate oxalates with a (4,6)-connected fsh topology. *Inorganic Chemistry*, **54**, 9387–9389.

Mandarino J.A. (2007) The Gladstone–Dale compatibility of minerals and its use in selecting mineral species for further study. *The Canadian Mineralogist*, **45**, 1307–1324.

Mills S.J., Birch W.D., Kampf A.R., Christy A. G., Pluth J.J., Pring A., Raudsepp M. and Chen Y. (2010a) Kapundaite, $(Na,Ca)_2Fe_4^{3+}(PO_4)_4(OH)_3\cdot 5H_2O$, a new phosphate species from Toms quarry, South Australia: description and structural relationship to mélonjosephite. *American Mineralogist*, **95**, 754–760.

Mills S.J., Kolitsch U., Miyawaki R., Hatert F., Porier G., Kampf A.R., Matsubara S. and Tillmanns E. (2010b) $Pb_3Fe_2^{3+}(PO_4)_4(H_2O)$, a new octahedral-tetrahedral framework structure with double-strand chains. *European Journal of Mineralogy*, **22**, 595–604.

Peterson K.I. and Pullman D.P. (2016) Determining the structure of oxalate anion using infrared and Raman spectroscopy coupled with Gaussian calculations. *Journal of Chemical Education*, **93**, 1130–1133.

Pouchou J.-L. and Pichoir F. (1991) Quantitative analysis of homogeneous or stratified microvolumes applying the model "PAP." Pp. 3l–75 in: *Electron Probe Quantitation* (K.F.J. Heinrich and D.E. Newbury, editors). Plenum Press, New York.

Sheldrick G.M. (2015) Crystal structure refinement with SHELX. *Acta Crystallographica*, **C71**, 3–8.

Wilson W.E. (2020) The Rowley mine, Painted Rock Mountains, Maricopa County, Arizona. *Mineralogical Record*, **51**, 181–226.